

NASA TECHNICAL NOTE



NASA TN D-3877

C.1

NASA TN D-3877

LOAN COPY: RETURN
AFWL (WJL-2)
Kirtland AFB, N.M.

0130609



TECH LIBRARY KAFB, NM

THE AXIALLY SYMMETRIC RESPONSE OF AN ELASTIC CYLINDRICAL SHELL PARTIALLY FILLED WITH LIQUID

by Richard M. Beam and LeRoy R. Guist

Ames Research Center

Moffett Field, Calif.

TECH LIBRARY KAFB, NM



0130609

THE AXIALLY SYMMETRIC RESPONSE OF AN ELASTIC CYLINDRICAL
SHELL PARTIALLY FILLED WITH LIQUID

By Richard M. Beam and LeRoy R. Guist

Ames Research Center
Moffett Field, Calif.

NATIONAL AERONAUTICS AND SPACE ADMINISTRATION

For sale by the Clearinghouse for Federal Scientific and Technical Information
Springfield, Virginia 22151 - Price \$2.00

THE AXIALLY SYMMETRIC RESPONSE OF AN ELASTIC CYLINDRICAL
SHELL PARTIALLY FILLED WITH LIQUID

By Richard M. Beam and LeRoy R. Guist
Ames Research Center

SUMMARY

The axially symmetric response of a circular cylindrical shell partially filled with a liquid and subjected to axial displacements and pressurization fluctuations is investigated analytically and experimentally. Two solutions are presented: one, an "exact" series solution and the other, an approximate solution. The correlation of theoretical and experimental results indicates that the theory presents a good mathematical model of the physical system and that the approximate solution is adequate for many practical problems.

INTRODUCTION

The use of liquid propellant for missiles and spacecraft launch vehicles introduces problems associated with the dynamics of liquid-filled shells. Initially, there were primarily control problems resulting from the "propellant sloshing" or motion of the liquid free surface. Later, however, as the size of propellant tanks was increased and the ratio of wall thickness to radius decreased, the coupling of the shell and liquid dynamics produced unexpected and undesirable oscillations of flight vehicles. In particular, the longitudinal oscillation resulting from the coupling of the liquid-shell system with the shell support structure and the tank pressurization system can influence the success of certain missions and can interfere with the comfort of astronauts in manned vehicles.

Several papers have been published on the dynamics of the coupled liquid-shell system (refs. 1-8). Most of these papers are limited to the anaxisymmetric oscillations generally predominant in flutter calculations. Those papers that consider the axisymmetric oscillations lack information required to analyze the complete vehicle, namely, (a) the equations and coefficients that couple the liquid-shell system and the shell support and pressurization systems, (b) approximate equations suitable for preliminary design calculations, and (c) experimental verification of the applicability of the theory.

The purpose of this report is to present a method for computing the response of a preloaded, thin circular cylindrical shell partially filled with a liquid and subjected to axial base displacements and applied pressure fluctuations in the liquid-free shell space. A general series solution is obtained for the natural frequencies of oscillation and normal modes. In addition, an approximate one-term solution applicable to very thin shells is presented. The equations coupling the motion of the liquid-shell system with

the base and pressure fluctuations are derived. Finally, a comparison is made between the two analytical solutions and experimental results.

SYMBOLS

A_{ms}	constant defined by equation (19)
$a_n(t)$	coefficient of series of modal functions
B_{mk}, C_j	constants defined by equation (19)
C_{1n}	constant defined by equation (29c)
D_m	constant defined by equation (19)
E	modulus of elasticity of shell material
e	dimensionless length of shell, $\frac{l}{R_0}$
h	depth of liquid in shell
I_0	modified Bessel function of the first kind
J_0	Bessel function of the first kind
j, k	integers
l	length of shell
m, n	integers
N_x	shell axial preload (i.e., axial shell loading for static condition)
\bar{N}_x	dimensionless shell axial preload, $\frac{N_x}{ER_0}$
P	force on bottom of shell
P_m	constant defined by equation (19)
p	pressure in region occupied by liquid (also used as integer subscript)
$p_0(t)$	pressure in liquid-free volume of shell
$\bar{p}_0(t)$	dimensionless pressure in liquid-free volume of shell, $\frac{p_0}{E}$
Q_k	constant defined by equation (19)

q	surface pressure on shell
R	cylindrical coordinate
\bar{R}	dimensionless cylindrical coordinate, $\frac{R}{R_0}$
R_0	radius of cylindrical shell
R_s	constant defined by equation (19)
r_n	coefficient of Fourier-Bessel series
s	integer
s_n, s_j^s	coefficients of Fourier sine series
t	time variable
u	axial displacement of shell bottom
\bar{u}	dimensionless axial displacement of shell bottom
w	radial displacement component of shell wall
\bar{w}	dimensionless radial displacement component of shell wall, $\frac{w}{R_0}$
x	cylindrical coordinate
Z_{1n}, Z_{2n}, Z_{3n}	coupling coefficients defined by equations (29a), (29b), and (33)
α	dimensionless cylindrical coordinate, $\frac{x}{R_0}$
β	dimensionless shell thickness, $\frac{\delta}{R_0}$
β_k	constant defined by equation (6b)
γ_n	dimensionless form of $\delta_n, \delta_n R_0$
δ	shell thickness
δ_n	constant defined by equation (6a)
ϵ	dimensionless liquid depth, $\frac{h}{R_0}$
η	integration variable
λ	step function defined by equation (15a)

μ	ratio of shell-material and liquid densities, $\frac{\rho_s}{\rho}$
ν	Poisson's ratio for shell material
ξ	integration variable
ρ	liquid mass density
ρ_s	shell-material mass density
σ	eigenvalue (frequency squared)
$\bar{\sigma}$	dimensionless form of σ , $\sigma \frac{R_0^2 \rho}{E}$
Φ	velocity potential function
Φ_s	modal function
Ψ	displacement potential function
ω_s	frequency of oscillation

ANALYSIS

The liquid-shell geometry and coordinate system are shown in figure 1. The analysis is restricted to small (linear) displacements that are symmetric about the axis of the cylinder. The liquid is incompressible and inviscid and the flow irrotational. The liquid is bounded at the bottom of the cylinder by a rigid flat surface, at the free surface by a light (negligible density) gas at pressure $p_0(t)$, and at the cylinder surface by the flexible shell wall. The shell has simply supported boundaries and is preloaded with a constant axial stress. Only the radial inertia of the shell is included in the analysis. All body forces acting on the liquid are assumed to be zero; therefore, the "sloshing" modes of the free surface do not appear in the mathematical model. In general, the body forces may be excluded from this type of analysis because of the low frequency spectrum of the sloshing modes relative to the liquid shell modes.

The analysis is divided into four parts: (a) equations of motion of the liquid, (b) coupling of the shell-liquid equations, (c) determination of natural frequencies and modes of oscillation, and (d) response of the liquid-shell system to displacement and pressure disturbances.

Equations of Motion of the Liquid

For irrotational flow of an incompressible liquid, the velocity potential Φ satisfies the continuity equation (ref. 9)

$$\nabla^2 \Phi = \left(\frac{\partial}{\partial R^2} + \frac{1}{R} \frac{\partial}{\partial R} + \frac{\partial^2}{\partial x^2} \right) \Phi = 0 \quad (1)$$

in the region occupied by the liquid ($0 \leq x \leq h$, $0 \leq R \leq R_0$). Since the liquid displacements at the shell are directly related to the shell wall displacements, it is convenient to use a displacement potential, Ψ (where $\Phi = \partial\Psi/\partial t$), rather than the velocity potential. In addition to being a harmonic function ($\nabla^2\Psi = 0$), Ψ must satisfy the following boundary conditions.

On the free surface ($x = h$), the pressure is a prescribed function [$p_0(t)$] of time

$$p \Big|_{x=h} = -\rho \frac{\partial^2 \Psi}{\partial t^2} \Big|_{x=h} = p_0(t) \quad (2)$$

where p is the pressure in the liquid and ρ is the liquid density.

At the shell bottom ($x = 0$), the liquid must have the same axial motion [$u(t)$] as the rigid tank bottom

$$\frac{\partial \Psi}{\partial x} \Big|_{x=0} = u(t) \quad (3)$$

The liquid adjacent to the shell wall ($R = R_0$) must move radially with the tank wall

$$\frac{\partial \Psi}{\partial R} \Big|_{R=R_0} = w(x,t) \quad (4)$$

where $w(x,t)$ is the shell-wall radial displacement component.

The displacement potential Ψ may be obtained by the method of separation of variables applied to the continuity equation ($\nabla^2\Psi = 0$). If the arbitrary constants resulting from the separation of variables are chosen so that boundary condition equations (3) and (4) are satisfied, the following function is found

$$\Psi(x, R, t) = r_0(t) + \sum_{n=1}^{\infty} r_n(t) \frac{\cosh \delta_n x}{\delta_n \sinh \delta_n h} \frac{J_0(\delta_n R)}{J_0(\delta_n R_0)} + \frac{1}{2hR_0} (R^2 - 2x^2) \int_0^h w(\xi, t) d\xi$$

$$+ \sum_{k=1}^{\infty} \left(\int_0^h w(\xi, t) \cos \beta_k \xi d\xi \right) \frac{2}{k\pi} \frac{I_0(\beta_k R)}{I_0'(\beta_k R_0)} \cos \beta_k x + xu(t) \quad (5)$$

where

$$J_0'(\delta_n R_0) = 0 \quad n = 0, 1, 2 \quad (6a)$$

$$\beta_k = \frac{k\pi}{h} \quad k = 1, 2 \quad (6b)$$

and J_0 and I_0 are Bessel functions and modified Bessel functions, respectively, of the first kind and zero order. The arbitrary functions of time, r_n , may be used to satisfy the remaining boundary condition (eq. (2)).

The value of r_n may be determined in the following manner. The function Ψ is substituted from equation (5) into the free surface boundary condition equation (2). The resulting equation is then multiplied by $RJ_0(\delta_n R)dR$ and integrated from zero to R_0 . After the appropriate algebraic manipulations, the following expressions for r_n result¹

¹The derivation of equations (7) and (8) is expedited by the following identities

$$(a) \quad \frac{1}{\beta_k^2} \cos \beta_k h = \frac{1}{2h} \int_0^h x^2 \cos \beta_k x dx$$

$$(b) \quad \int_0^h \ddot{w}(x, t) x^2 dx = \frac{h^2}{3} \int_0^h \ddot{w}(x, t) dx$$

$$+ \frac{2}{h} \sum_{k=1}^{\infty} \left[\int_0^h \ddot{w}(x, t) \cos \beta_k x dx \right] \left(\int_0^h x^2 \cos \beta_k x dx \right)$$

$$(c) \quad \frac{\cos \beta_k h}{\beta_k^2 + \delta_s^2} = \frac{1}{\delta_s \sinh \delta_s h} \int_0^h \cos \beta_k x \cosh \delta_s x dx$$

$$(d) \quad \int_0^h \ddot{w}(x, t) \cosh \delta_s x dx = \frac{\sinh \delta_s h}{\delta_s h} \int_0^h \ddot{w}(x, t) dx$$

$$+ \frac{2}{h} \sum_{k=1}^{\infty} \left[\int_0^h \ddot{w}(x, t) \cos \beta_k x dx \right] \left(\int_0^h \cosh \delta_k x \cos \beta_k x dx \right)$$

$$\ddot{r}_0(t) = \left[-\frac{1}{4} \frac{R_0}{h} \int_0^h \ddot{w}(\xi, t) d\xi + \frac{4}{3} \frac{h}{R_0} \int_0^h \ddot{w}(\xi, t) d\xi - \frac{1}{hR_0} \int_0^h \ddot{w}(\xi, t) \xi^2 d\xi \right] - h\ddot{u}(t) - \frac{p_0(t)}{\rho} \quad (7)$$

$$\ddot{r}_s(t) = -\frac{2}{R_0 \cosh \delta_s h} \int_0^h \ddot{w}(\xi, t) \cosh \delta_s \xi d\xi \quad (8)$$

The pressure in the fluid may now be expressed as a function of the shell-wall displacement, the free-surface pressure, and the axial motion of the shell bottom:

$$\begin{aligned} \frac{p(x, R, t)}{\rho} = & \sum_{n=1}^{\infty} \frac{2}{R_0} \frac{\cosh \delta_n x}{\delta_n \sinh \delta_n h \cosh \delta_n h} \left[\int_0^h \ddot{w}(\xi, t) \cosh \delta_n \xi d\xi \right] \frac{J_0(\delta_n R)}{J_0(\delta_n R_0)} \\ & + \frac{1}{4} \frac{R_0}{h} \int_0^h \ddot{w}(\xi, t) d\xi - \frac{4}{3} \frac{h}{R_0} \int_0^h \ddot{w}(\xi, t) d\xi + \frac{1}{hR_0} \int_0^h \ddot{w}(\xi, t) \xi^2 d\xi \\ & - \frac{1}{2hR_0} (R^2 - 2x^2) \int_0^h \ddot{w}(\xi, t) d\xi \\ & - \sum_{k=1}^{\infty} \left[\int_0^h \ddot{w}(\xi, t) \cos \beta_k \xi d\xi \right] \frac{2}{k\pi} \frac{I_0(\beta_k R)}{I_0'(\beta_k R_0)} \cos \beta_k x - (x - h)\ddot{u}(t) \\ & + \frac{p_0(t)}{\rho} \end{aligned} \quad (9)$$

It is worthwhile to note that the expression for the pressure does not depend on the shell boundary conditions and, accordingly, is applicable for the analysis that includes any shell boundary conditions.

The liquid pressure, q , acting on the shell is obtained from $q = p(x, R_0, t)$

$$\begin{aligned}
\frac{q(x,t)}{\rho} = & \sum_{n=1}^{\infty} \frac{2}{R_0} \frac{\cosh \delta_n x}{\delta_n \sinh \delta_n h \cosh \delta_n h} \left[\int_0^h \ddot{w}(\xi,t) \cosh \delta_n \xi \, d\xi \right] - \frac{1}{4} \frac{R_0}{h} \int_0^h \ddot{w}(\xi,t) \, d\xi \\
& - \frac{1}{3} \frac{h}{R_0} \int_0^h \ddot{w}(\xi,t) \, d\xi + \frac{1}{h R_0} \int_0^h \ddot{w}(\xi,t) \xi^2 \, d\xi + \frac{1}{h R_0^2} x^2 \int_0^h \ddot{w}(\xi,t) \, d\xi \\
& - \sum_{k=1}^{\infty} \left[\int_0^h \ddot{w}(\xi,t) \cos \beta_k \xi \, d\xi \right] \frac{2}{k\pi} \frac{I_0(\beta_k R_0)}{I_0'(\beta_k R_0)} \cos \beta_k x - (x-h)\ddot{u}(t) \\
& + \frac{1}{\rho} p_0(t) \quad 0 \leq x \leq h
\end{aligned} \tag{10}$$

With the dimensionless parameters,

$$\left. \begin{aligned}
\bar{R} = \frac{R}{R_0}, \quad \alpha = \frac{x}{R_0}, \quad \eta = \frac{\xi}{R_0}, \quad e = \frac{l}{R_0}, \\
\epsilon = \frac{h}{R_0}, \quad \bar{u} = \frac{u}{R_0}, \quad \gamma_n = \delta_n R_0, \quad \bar{w} = \frac{w}{R_0}
\end{aligned} \right\} \tag{11}$$

equation (10) may be rewritten

$$\begin{aligned}
\frac{q}{\rho R_0^2} = & \sum_{n=1}^{\infty} \frac{2}{\gamma_n} \frac{\cosh \gamma_n \alpha}{\sinh \gamma_n \epsilon \cosh \gamma_n \epsilon} \left[\int_0^\epsilon \ddot{\bar{w}}(\eta,t) \cosh \gamma_n \eta \, d\eta \right] \\
& - \left(\frac{1}{4\epsilon} + \frac{1}{3} \epsilon \right) \int_0^\epsilon \ddot{\bar{w}}(\eta,t) \, d\eta + \frac{1}{\epsilon} \left[\int_0^\epsilon \ddot{\bar{w}}(\eta,t) \eta^2 \, d\eta + \alpha^2 \int_0^\epsilon \ddot{\bar{w}}(\eta,t) \, d\eta \right] \\
& - \sum_{k=1}^{\infty} \left[\int_0^\epsilon \ddot{\bar{w}}(\eta,t) \cos \frac{k\pi}{\epsilon} \eta \, d\eta \right] \frac{2}{k\pi} \frac{I_0(k\pi/\epsilon)}{I_0'(k\pi/\epsilon)} \cos \frac{k\pi}{\epsilon} \alpha - (\alpha - \epsilon)\ddot{\bar{u}}(t) + \frac{p_0(t)}{R_0^2 \rho}
\end{aligned} \tag{12}$$

Equations of Motion of the Shell

If a circular cylindrical shell of uniform thickness, δ , is subjected to a constant axial load,² N_x , uniformly distributed around the circumference, and an axially symmetric surface load, $q(x,t)$, the differential equation for the radial deflection component w (ref. 10) is

$$\frac{E\delta^3}{12(1-\nu^2)} \frac{\partial^4 w}{\partial x^4} - N_x \frac{\partial^2 w}{\partial x^2} + \frac{E\delta}{R_0^2} w = -\rho_s \frac{\partial^2 w}{\partial t^2} \delta + q(x,t) \quad (13)$$

where E , ν , δ , and ρ_s are the modulus of elasticity, Poisson's ratio, thickness, and density of the shell material.

With the dimensionless notation

$$\beta = \frac{\delta}{R_0}, \quad \bar{N}_x = \frac{N_x}{ER_0}, \quad \mu = \frac{\rho_s}{\rho} \quad (14)$$

and $q(x,t)$ from equation (12), the shell equation may be written

$$\begin{aligned} & \frac{\beta^3}{12(1-\nu^2)} \frac{\partial^4 \bar{w}}{\partial \alpha^4} - \bar{N}_x \frac{\partial^2 \bar{w}}{\partial \alpha^2} + \beta \bar{w} \\ &= \frac{R_0^2 \rho}{E} \left(-\mu \beta \ddot{\bar{w}}(\alpha, t) + \lambda(\alpha) \left\{ \sum_{n=1}^{\infty} 2 \frac{\cosh \gamma_n \alpha}{\gamma_n \sinh \gamma_n \epsilon \cosh \gamma_n \epsilon} \left[\int_0^\epsilon \ddot{\bar{w}}(\eta, t) \cosh \gamma_n \eta \, d\eta \right] \right. \right. \\ & \quad \left. \left. - \left(\frac{1}{4\epsilon} + \frac{4\epsilon}{3} \right) \int_0^\epsilon \ddot{\bar{w}}(\eta, t) \, d\eta + \frac{1}{\epsilon} \left[\int_0^\epsilon \ddot{\bar{w}}(\eta, t) \eta^2 \, d\eta + \alpha^2 \int_0^\epsilon \ddot{\bar{w}}(\eta, t) \, d\eta \right] \right. \right. \\ & \quad \left. \left. - \sum_{k=1}^{\infty} \left[\int_0^\epsilon \ddot{\bar{w}}(\eta, t) \cos \frac{k\pi}{\epsilon} \eta \, d\eta \right] \frac{2}{k\pi} \frac{I_0(k\pi/\epsilon)}{I_1(k\pi/\epsilon)} \cos \frac{k\pi}{\epsilon} \alpha - (\alpha - \epsilon) \ddot{u}(t) \right\} + \frac{p_0(t)}{\rho R_0^2} \right) \quad (15) \end{aligned}$$

²The value N_x is determined from the static loading condition, that is, from any constant pressure in the shell plus axial loads applied to the ends of the shell. It is assumed that the variation of axial loading resulting from $p_0(t)$ and $u(t)$ produces negligible variations of N_x (i.e., $N_x = \text{constant}$).

where

$$\lambda(\alpha) = \begin{cases} 1 & 0 \leq \alpha \leq e \\ 0 & \alpha > e \end{cases} \quad (15a)$$

For simply supported boundary conditions, the shell displacement and its derivatives must satisfy the following equations:

$$\bar{w}(0) = \bar{w}''(0) = \bar{w}(e) = \bar{w}''(e) = 0 \quad (16)$$

where

$$\frac{\partial}{\partial \alpha} \bar{w} = \bar{w}'$$

Shell-Liquid Natural Frequencies and Modes of Oscillation

The shell-wall response to base displacements and pressure fluctuations is the function \bar{w} which satisfies equations (15) and (16) plus the initial conditions. This response, which can be used to evaluate the desired coupling characteristics is obtained in the following manner. First, a series solution for the homogeneous part of equation (15) ($p_0 = \bar{u} = 0$) will be obtained by assuming that the time variation of \bar{w} is proportional to $\exp(i\sqrt{\sigma} t)$. This will result in a set of eigenfunctions $\varphi_s(\alpha)$ that can be used in computing the response $\bar{w}(\alpha, t)$ to the disturbances p_0 and \bar{u} (i.e., the nonhomogeneous eq. (15)). In this manner, let

$$\bar{w} = \sum_{j=1}^{\infty} s_j \sin \frac{j\pi}{e} \alpha \exp(i\sqrt{\sigma} t) \quad (17)$$

and substitute into equation (15). The equations for the coefficients s_j are obtained by multiplying the resulting equation by $\sin(m\pi/e)\alpha d\alpha$ and integrating from zero to e . The following set of simultaneous equations results:

$$\left[\frac{\beta^3}{12(1-\nu^2)} \left(\frac{m\pi}{e} \right)^4 + \bar{N}_x \left(\frac{m\pi}{e} \right)^2 + \beta \right] \frac{1}{2} s_m$$

$$= -\frac{R_0^2 \rho \sigma}{E} \left\{ -\beta \mu \frac{1}{2} s_m + \sum_{n=1}^{\infty} 2 \left(\int_0^{\epsilon} \sum_{j=1}^{\infty} s_j \sin \frac{j\pi}{e} \eta \cosh \gamma_n \eta \, d\eta \right) \frac{\int_0^{\epsilon} \sin \frac{m\pi}{e} \alpha \cosh \gamma_n \alpha \, d\alpha}{\gamma_n \sinh \gamma_n \epsilon \cosh \gamma_n \epsilon} \right.$$

$$- \left(\frac{1}{4\epsilon} + \frac{4\epsilon}{3} \right) \left(\int_0^{\epsilon} \sum_{j=1}^{\infty} s_j \sin \frac{j\pi}{e} \eta \, d\eta \right) \int_0^{\epsilon} \sin \frac{m\pi}{e} \alpha \, d\alpha$$

$$+ \frac{1}{\epsilon} \left[\int_0^{\epsilon} \sum_{j=1}^{\infty} s_j \left(\sin \frac{j\pi \eta}{e} \right) \eta^2 \, d\eta \int_0^{\epsilon} \sin \frac{m\pi \alpha}{e} \, d\alpha \right.$$

$$+ \left. \int_0^{\epsilon} \sum_{j=1}^{\infty} s_j \sin \frac{j\pi \eta}{e} \, d\eta \int_0^{\epsilon} \alpha^2 \sin \frac{m\pi \alpha}{e} \, d\alpha \right]$$

$$- \sum_{k=1}^{\infty} \left(\int_0^{\epsilon} \sum_{j=1}^{\infty} s_j \sin \frac{j\pi \eta}{e} \cos \frac{k\pi}{\epsilon} \eta \, d\eta \right) \frac{2}{k\pi} \frac{I_0(k\pi/\epsilon)}{I_0'(k\pi/\epsilon)} \int_0^{\epsilon} \sin \frac{m\pi \alpha}{e} \cos \frac{k\pi}{\epsilon} \alpha \, d\alpha \left. \right\}$$

$$m = 1, 2, 3, \dots, \infty \quad (18)$$

With the definitions

$$\begin{aligned}
 A_{ms} &= \left(\int_0^\epsilon \sin \frac{m\pi}{e} \alpha \cosh \gamma_s \alpha \, d\alpha \right) (\cosh \gamma_s \epsilon)^{-1} \\
 B_{mk} &= \int_0^\epsilon \sin \frac{m\pi}{e} \alpha \cos \frac{k\pi}{e} \alpha \, d\alpha \\
 C_j &= \int_0^\epsilon \sin \frac{j\pi}{e} \eta \, d\eta \\
 D_m &= \int_0^\epsilon \alpha^2 \sin \frac{m\pi \alpha}{e} \, d\alpha \\
 E_j &= \int_0^\epsilon \alpha \sin \frac{j\pi \alpha}{e} \, d\alpha \\
 P_m &= \frac{\beta^3}{12(1 - \nu^2)} \left(\frac{m\pi}{e} \right)^4 + \bar{N}_x \left(\frac{m\pi}{e} \right)^2 + \beta \\
 Q_k &= \frac{2}{k} \frac{I_0(k\pi/\epsilon)}{I_0'(k\pi/\epsilon)} \\
 R_s &= \frac{1}{\gamma_s \tanh \gamma_s \epsilon} \\
 \bar{\sigma} &= \frac{R_0^2 \rho \sigma}{E}
 \end{aligned} \tag{19}$$

equation (18) can be simplified to

$$\begin{aligned}
 \left(P_m \frac{e}{2} \right) s_m + \bar{\sigma} \left\{ - \left(\mu \beta \frac{e}{2} \right) s_m + \sum_{j=1}^{\infty} \left[2 \sum_{n=1}^{\infty} A_{jn} A_{mn} R_n - \left(\frac{1}{4} \frac{1}{e} + \frac{4}{3} e \right) C_j C_m \right. \right. \\
 \left. \left. + \frac{1}{e} (D_j C_m + C_j D_m) - \sum_{k=1}^{\infty} B_{jk} B_{mk} Q_k \right] s_j \right\} = 0 \quad m = 1, 2, 3, \dots \tag{20}
 \end{aligned}$$

The simultaneous equations (20) are homogeneous and therefore have a non-trivial solution only if the determinant of the coefficients of s_j vanish. This provides the eigenvalue problem for the eigenvalues $\bar{\sigma}_s$ and the corresponding eigenfunctions s_j^s which, in turn, lead to the modal functions φ_s

$$\varphi_s = \sum_{j=1}^{\infty} s_j^s \sin \frac{j\pi}{e} \alpha \quad (21)$$

The natural frequency of oscillation of the mode φ_s is related to $\bar{\sigma}_s$ by

$$\omega_s = \sqrt{\frac{\bar{\sigma}_s E}{R_0 2 \rho}} = \sqrt{\bar{\sigma}_s} \quad (22)$$

where ω_s is in radians per unit time.

Response to Pressure and Displacement Fluctuations

With the aid of the modal functions obtained in the previous section, the solution to equation (15) may be expressed as

$$\bar{w}(x,t) = \sum_{n=1}^{\infty} a_n(t) \varphi_n(\alpha) \quad (23)$$

where a_n is as yet an undetermined function of time. The differential equations for evaluating a_n are obtained by substituting \bar{w} from equation (23) into equation (15), multiplying the resulting equation by $\varphi_m(\alpha) d\alpha$, and integrating from zero to e , which produces

$$\begin{aligned}
& \int_0^\epsilon \sum_{n=1}^{\infty} \left[\frac{\beta^3}{12(1-\nu^2)} \frac{\partial^4 \varphi_n}{\partial \alpha^4} - N_x \frac{\partial^2 \varphi_n}{\partial \alpha^2} + \beta \varphi_n \right] a_n(t) \varphi_m \, d\alpha \\
&= \frac{R_0^2 \rho}{E} \left(-\mu \beta \int_0^\epsilon \sum_{n=1}^{\infty} \ddot{a}_n(t) \varphi_n \varphi_m \, d\alpha \right. \\
&+ \left. \left\{ \int_0^\epsilon \sum_{p=1}^{\infty} 2 \frac{(\cosh \gamma_p \alpha) \varphi_m(\alpha) \, d\alpha}{\gamma_p \sinh \gamma_p \epsilon \cosh \gamma_p \epsilon} \left[\int_0^\epsilon \sum_{n=1}^{\infty} \ddot{a}_n(t) \varphi_n \cosh \gamma_p \eta \, d\eta \right] \right. \right. \\
&- \left. \left. \left(\frac{1}{4\epsilon} + \frac{4}{3} \epsilon \right) \left[\int_0^\epsilon \sum_{n=1}^{\infty} \ddot{a}_n(t) \varphi_n \, d\eta \right] \left[\int_0^\epsilon \varphi_m(\alpha) \, d\alpha \right] \right. \right. \\
&- \left. \left. \sum_{k=1}^{\infty} \left[\int_0^\epsilon \sum_{n=1}^{\infty} \ddot{a}_n(t) \varphi_n \cos \frac{k\pi}{\epsilon} \eta \, d\eta \right] \frac{2}{k\pi} \frac{I_0\left(\frac{k\pi}{\epsilon}\right)}{I_0'\left(\frac{k\pi}{\epsilon}\right)} \int_0^\epsilon \varphi_m \cos \frac{k\pi \alpha}{\epsilon} \, d\alpha \right. \right. \\
&- \left. \left. \int_0^\epsilon (\alpha - \epsilon) \varphi_m \, d\alpha \ddot{u}(t) + \frac{p_0(t)}{\rho R_0^2} \int_0^\epsilon \varphi_m \, d\alpha + \frac{1}{\epsilon} \left[\int_0^\epsilon \sum_{n=1}^{\infty} \ddot{a}_n(t) \varphi_n \eta^2 \, d\eta \int_0^\epsilon \varphi_m \, d\alpha \right. \right. \right. \\
&+ \left. \left. \left. \int_0^\epsilon \sum_{n=1}^{\infty} \ddot{a}_n(t) \varphi_n \, d\eta \int_0^\epsilon \alpha^2 \varphi_m \, d\alpha \right] \right\} \right) \quad (24)
\end{aligned}$$

With the aid of equations (15) and (16) and the properties of the eigenfunctions of the previous section, the following orthogonality relationships can be derived:

$$\begin{aligned}
& -\mu\beta \int_0^\epsilon \varphi_n \varphi_m \, d\alpha + \left[\sum_{s=1}^{\infty} 2 \frac{\int_0^\epsilon \varphi_n \cosh \gamma_s \eta \, d\eta \int_0^\epsilon (\cosh \gamma_s \alpha) \varphi_m \, d\alpha}{\gamma_s \cosh \gamma_s \epsilon \sinh \gamma_s \epsilon} - \left(\frac{1}{4\epsilon} + \frac{4\epsilon}{3} \right) \right. \\
& \int_0^\epsilon \varphi_n \, d\eta \int_0^\epsilon \varphi_m \, d\alpha + \frac{1}{\epsilon} \left(\int_0^\epsilon \varphi_m \alpha^2 \, d\alpha \int_0^\epsilon \varphi_n \, d\eta + \int_0^\epsilon \varphi_n \eta^2 \, d\eta \int_0^\epsilon \varphi_m \, d\alpha \right) \\
& \left. - \sum_{k=1}^{\infty} \left(\int_0^\epsilon \varphi_m \cos \frac{k\pi}{\epsilon} \eta \right) \frac{2}{k\pi} \frac{I_0(k\pi/\epsilon)}{I_0'(k\pi/\epsilon)} \int_0^\epsilon \varphi_n \cos \frac{k\pi}{\epsilon} \alpha \, d\alpha \right] = 0 \quad m \neq n \quad (25)
\end{aligned}$$

$$\int_0^\epsilon \left[\frac{\beta^3}{12(1-\nu^2)} \frac{\partial^4 \varphi_n}{\partial \alpha^4} - \bar{N}_x \frac{\partial^2 \varphi_n}{\partial \alpha^2} + \beta \varphi_n \right] \varphi_m \, d\alpha = 0 \quad m \neq n \quad (26)$$

and

$$\begin{aligned}
& \int_0^\epsilon \left[\frac{\beta^3}{12(1-\nu^2)} \frac{\partial^4 \varphi_n}{\partial \alpha^4} - N_x \frac{\partial^2 \varphi_n}{\partial \alpha^2} + \beta \varphi_n \right] \varphi_m \, d\alpha \\
& = \sum_{j=1}^{\infty} \left[\frac{\beta^3}{12(1-\nu^2)} \left(\frac{j\pi}{\epsilon} \right)^4 + \bar{N}_x \left(\frac{j\pi}{\epsilon} \right)^2 + \beta \right] (s_j^n)^2 \frac{\epsilon}{2} \quad m = n \quad (27)
\end{aligned}$$

The differential equation for $a_n(t)$ (eq. (24)) may be simplified to

$$\ddot{a}_n(t) + \omega_n^2 a_n(t) = Z_{1n} \ddot{u}(t) + Z_{2n} \bar{p}_0(t) \quad (28)$$

where

$$Z_{1n} = \frac{\bar{\sigma}_n}{C_{1n}} \int_0^\epsilon (\alpha - \epsilon) \varphi_n(\alpha) \, d\alpha = - \frac{\bar{\sigma}_n}{C_{1n}} \left[\sum_{j=1}^{\infty} (E_j - \epsilon C_j) s_j^n \right] \quad (29a)$$

$$Z_{2n} = \frac{\omega_n^2}{C_{1n}} \int_0^\epsilon \varphi_n(\alpha) \, d\alpha = \frac{\omega_n^2}{C_{1n}} \left\{ \sum_{j=1}^{\infty} \frac{\epsilon}{j\pi} [(-1)^j - 1] s_j^n \right\} \quad (29b)$$

$$C_{1n} = \sum_{j=1}^{\infty} \left[\frac{\beta^3}{12(1-\nu^2)} \left(\frac{j\pi}{e} \right)^4 + \bar{N}_x \left(\frac{j\pi}{e} \right)^2 + \beta \right] (s_j^n)^2 \frac{e}{2} \quad (29c)$$

$$\bar{p}_o(t) = \frac{p_o(t)}{E} \quad (30)$$

If the disturbances \bar{u} and \bar{p}_o are prescribed, the shell response is readily obtained from equations (23) and (28). The coupling of the liquid-shell system and the shell-support system requires, in addition, the axial force acting on the bottom of the shell. The pressure in the fluid as a function of a_n is obtained by the substitution of \bar{w} from equation (23) into the pressure equation (9).

$$\begin{aligned} \frac{p(\alpha, \bar{R}, t)}{\rho R_o^2} = & \sum_{p=1}^{\infty} \ddot{a}_p \left\{ \sum_{n=1}^{\infty} 2 \frac{\cosh \gamma_n \alpha}{\gamma_n \sinh \gamma_n \epsilon} \frac{J_o(\gamma_n \bar{R})}{J_o(\gamma_n)} \sum_m^{\infty} A_{mn} s_m^p \right. \\ & - \left[-\frac{1}{4\epsilon} + \frac{4}{3\epsilon} + \frac{1}{2\epsilon} (\bar{R}^2 - 2\alpha^2) \right] \sum_m^{\infty} C_m s_m^p + \frac{1}{\epsilon} \sum_m^{\infty} D_m s_m^p \\ & \left. - \sum_k^{\infty} \frac{2}{k\pi} \frac{I_o[(k\pi/\epsilon)\bar{R}]}{I_o'(k\pi/\epsilon)} \cos \frac{k\pi}{\epsilon} \alpha \sum_m^{\infty} B_{mk} s_m^p \right\} - (\alpha - \epsilon) \ddot{u}(t) + \bar{p}_o(t) \frac{E}{\rho R_o^2} \end{aligned} \quad (31)$$

The total force, P , acting on the bottom of the shell is $\int p(o, \bar{R}, t) dA$, where the integral is over the area of the shell bottom; therefore,

$$P = \rho \pi R_o^4 \left[\sum_{p=1}^{\infty} 2Z_{3p} \ddot{a}_p + \frac{1}{\rho R_o^2} p_o(t) + \epsilon \ddot{u}(t) \right] \quad (32)$$

where

$$Z_{3p} = -\frac{2}{3\epsilon} \sum_{m=1}^{\infty} C_m s_m^p + \frac{1}{2\epsilon} \sum_{m=1}^{\infty} D_m s_m^p - \sum_{k=1}^{\infty} \frac{2\epsilon}{(k\pi)^2} \sum_{m=1}^{\infty} B_{mk} s_m^p \quad (33)$$

The coupling of the liquid-shell system and the shell-support and pressurization system is thus provided by equations (28) and (32). The coefficients Z_1 , Z_2 , and Z_3 will be called "coupling coefficients" in the discussion to follow.

Approximate solution (thin shells). - The complexity of the frequency equation and coupling coefficients in the previous sections makes that solution unattractive for preliminary design or analysis of a system. Since most liquid-shell systems used in missile and spacecraft construction have very thin wall shells, an approximate membrane solution of respectable accuracy can be expected. For thin shells subjected to loading that changes only gradually over the shell surface, the bending rigidity may be neglected in the interior of the shell. In addition, for the liquid-shell system under consideration, the shell boundary conditions (eq. (16)) may also be neglected since their influence is localized near the boundary.

A displacement potential satisfying the fluid boundary conditions equations (2), (3), and (4) is

$$\Psi = (x - h)u(t) - \frac{1}{\rho} \int_0^t \int_0^t p_0(t) dt_2 dt_1 + \sum_{k=1}^{\infty} \frac{2 \int_0^h w(\xi, t) \cos \beta_k \xi d\xi}{h I_0'(\beta_k R_0) \beta_k} \cos(\beta_k x) I_0(\beta_k R) \quad (5')$$

where

$$\beta_k = \left(k - \frac{1}{2}\right) \frac{\pi}{h} \quad (6b')$$

Note that β_k , as defined by equation (6b'), differs from the β_k of equation (6b). The simplification of the displacement potential and thus the new definition of β results from the relaxation of the boundary conditions on the shell and the lack of shell bending rigidity, that is, the displacement w at $x = 0$, is not required to be zero and, in addition, it is known a priori that the shell displacement, w , will be zero at the free surface ($x = h$).

The pressure in the liquid is

$$\frac{p}{\rho} = -(x - h)\ddot{u} + \frac{1}{\rho} p_0(t) - \sum_{k=1}^{\infty} \frac{2 \int_0^h \ddot{w}(\xi, t) \cos \beta_k \xi d\xi}{h I_0'(\beta_k R_0) \beta_k} \cos(\beta_k x) I_0(\beta_k R) \quad (9')$$

and the surface loading $q(x, t)$ on the shell is

$$\frac{q(\alpha, t)}{\rho R_0^2} = (\alpha - \epsilon)\ddot{u} - \frac{1}{\rho R_0^2} p_0(t) - \sum_{k=1}^{\infty} \frac{2}{\left(k - \frac{1}{2}\right)\pi} \frac{I_0\left[\left(k - \frac{1}{2}\right) \frac{\pi}{\epsilon}\right]}{I_0'\left(k - \frac{1}{2}\right) \frac{\pi}{\epsilon}} \int_0^\epsilon \ddot{w}(\eta, t) \cos\left[\left(k - \frac{1}{2}\right) \frac{\pi}{\epsilon} \eta\right] d\eta \cos\left[\left(k - \frac{1}{2}\right) \frac{\pi}{\epsilon} \alpha\right] \quad (12')$$

The equation for the shell-wall displacement \bar{w} (neglecting shell bending rigidity) is

$$-\bar{N}_x \frac{\partial^2 \bar{w}}{\partial \alpha^2} + \beta \bar{w} = \frac{R_0^2 \rho}{E} \left\{ -\mu \beta \ddot{\bar{w}} + \frac{1}{\rho R^2} p_0(t) - (\alpha - \epsilon) \ddot{u} - \sum_{k=1}^{\infty} \frac{2}{\left(k - \frac{1}{2}\right)\pi} \frac{I_0 \left[\left(k - \frac{1}{2}\right) \frac{\pi}{\epsilon} \right]}{I_0' \left[\left(k - \frac{1}{2}\right) \frac{\pi}{\epsilon} \right]} \int_0^{\epsilon} \ddot{w}(\eta, t) \cos \left[\left(k - \frac{1}{2}\right) \frac{\pi}{\epsilon} \eta \right] d\eta \cos \left[\left(k - \frac{1}{2}\right) \frac{\pi}{\epsilon} \alpha \right] \right\} \quad (15')$$

The frequency equation is obtained by substituting

$$\bar{w} = s_j \cos \left[\left(j - \frac{1}{2}\right) \pi \frac{\alpha}{\epsilon} \right] \exp(i\sqrt{\sigma} t) \quad (17')$$

into the homogeneous part of equation (15') (i.e., $p_0 = \bar{u} = 0$)

$$\left\{ \bar{N}_x \left[\left(j - \frac{1}{2}\right) \frac{\pi}{\epsilon} \right]^2 + \beta \right\} - \bar{\sigma} \left\{ \mu \beta + \frac{\epsilon}{j - \frac{1}{2}} \frac{I_0 \left[\left(j - \frac{1}{2}\right) \frac{\pi}{\epsilon} \right]}{I_0' \left[\left(j - \frac{1}{2}\right) \frac{\pi}{\epsilon} \right]} \right\} = 0$$

or

$$\bar{\sigma}_j = \frac{\bar{N}_x \left[\left(j - \frac{1}{2}\right) \frac{\pi}{\epsilon} \right]^2 + \beta}{\mu \beta + \frac{\epsilon}{\left(j - \frac{1}{2}\right)\pi} \frac{I_0 \left[\left(j - \frac{1}{2}\right) \frac{\pi}{\epsilon} \right]}{I_0' \left[\left(j - \frac{1}{2}\right) \frac{\pi}{\epsilon} \right]}} \quad (20')$$

The frequency equation is thus reduced to a single equation as opposed to the infinite determinant of the previous solution where the shell boundary conditions were included.

The response of the shell wall can be expressed in terms of the modal functions $\varphi_j = \cos \left[\left(j - \frac{1}{2}\right) \pi \frac{\alpha}{\epsilon} \right]$ as

$$\bar{w} = \sum_{n=1}^{\infty} a_n(t) \cos \left[\left(n - \frac{1}{2}\right) \pi \frac{\alpha}{\epsilon} \right] \quad (23')$$

The equations for a_n are obtained by substitution of \bar{w} from equation (23') into equation (15'), multiplication of the resulting equation by

$\cos \left[\left(m - \frac{1}{2}\right) \pi \frac{\alpha}{\epsilon} \right] d\alpha$ and integration over the interval zero to ϵ

$$\ddot{a}_m(t) + \omega_m^2 a_m(t) = Z_{1m} \ddot{u}(t) + Z_{2m} \bar{p}_0(t) \quad (28')$$

where

$$Z_{1m} = \frac{\bar{\sigma}_m}{C_{1m}} \frac{1}{\left[\left(m - \frac{1}{2} \right) \frac{\pi}{\epsilon} \right]^2} \quad (29a')$$

$$Z_{2m} = - \frac{\omega_m^2}{C_{1m}} \frac{\epsilon}{\left(m - \frac{1}{2} \right) \pi} (-1)^m \quad (29b')$$

$$C_{1m} = \left\{ \bar{N}_x \left[\left(m - \frac{1}{2} \right) \frac{\pi}{\epsilon} \right] + \beta \right\} \frac{\epsilon}{2} \quad (29c')$$

The total force on the shell bottom $P = \int_0^1 \int_0^{2\pi} p(0, \bar{R}, t) \bar{R} \, d\theta \, d\bar{R}$ is

$$P = \rho \pi R_0^4 \left[\sum_{p=1}^{\infty} 2Z_{3p} \ddot{a}_p + \frac{1}{\rho R_0^2} p_0(t) + \epsilon \ddot{u}(t) \right] \quad (32')$$

where

$$Z_{3p} = - \frac{1}{\left[\left(p - \frac{1}{2} \right) \frac{\pi}{\epsilon} \right]^2} \quad (33')$$

The frequency equation and coupling coefficients of this approximate solution are obviously more tractable than those of the series solution. The accuracy and applicability of the two solutions will be discussed further in the succeeding sections.

COMPARISON OF SERIES AND APPROXIMATE SOLUTIONS

This section presents the results of a brief numerical investigation designed to illustrate the convergence of the series solution and to compare the series and approximate solutions. First, the convergence of the series solution with increasing size of the frequency determinant is illustrated and compared with the approximate solution. Next, the convergence of the series solution with increasing shell thickness-to-radius ratio is considered, and, finally, the mode shapes and coupling coefficients from the two solutions are compared. Shells with large radius-to-thickness ratios (i.e., thin shells) were selected for the examples since the series solution rate of convergence (with frequency determinant size) should be slowest in these instances. The following discussion is limited to the first (lowest) two frequencies since

these are generally of primary concern to the analyst. The accuracy of the two solutions (as compared with experiment) will be discussed in the next section.

Frequency Parameters

The series solution frequency equation (determinant of coefficients of eq. (20) equated to zero) was approximated with various numbers of rows (m) and columns (j) ($m = j$) for a liquid-shell system with the following properties:

$$e = 2.4$$

$$\epsilon = 2.0$$

$$\bar{N}_x = 0.286 \times 10^{-6}$$

$$\nu = 0.3$$

$$\mu = 8.6$$

$$\beta = 0.00044, 0.044$$

The eigenvalues and eigenvectors of the resulting frequency equation were obtained with the aid of a digital computer using the threshold Jacobi eigenvalue routine. The variation of frequency parameter with determinant size is shown graphically in figure 2. The first and second mode frequency parameters ($\bar{\sigma}/\beta$) are shown for two values of shell thickness-to-radius ratio (β). Note that the second mode frequency "jumps" as the size of the determinant is increased from $M = 11$ to $m = 13$ and, correspondingly, the perturbation of the first mode frequency parameter plot is slight (almost undetectable in the figure) in the same region. Examination of the mode shapes reveals that this discontinuity is possibly a result of convergence to an "incorrect" second mode (i.e., lack of sufficient terms in the series to adequately describe the second mode) if $m < 13$.

For the thinner shells ($\beta = 0.00044$) the gradient of the shell-wall displacement should be very large in the vicinity of the shell bottom and, therefore, a slow convergence of the mode shape and frequency would be expected (due to the behavior of the sine series solution for $\alpha = 0$). As the shell thickness is increased, the convergence should improve. This is borne out by the frequency parameter plot (fig. 2) for the shell 100 times the thickness ($\beta = 0.04$) of the thinner shell. The approximate solution for the two shells is shown in figure 3. Note that for the thinner shell the difference between the two solutions is less than 2 percent for the first mode and 6 percent for the second mode. Even for the thicker shell ($\beta = 0.04$) the discrepancy between the series and approximate solution frequency parameter is less than 5 percent for the first and second modes.

MODE SHAPES

The mode shapes corresponding to the previous shell parameters are shown in figure 3. (The results for the approximate solution are indistinguishable for $\beta = 0.044$, $\beta = 0.00044$.) Here again the improvement of convergence of the series solution with increasing shell thickness is demonstrated. The first mode shape is, in fact, probably better represented by the approximate solution than by the series solution for $\alpha > 0$.

Coupling Coefficients

The natural frequencies and coupling coefficients are of primary importance in the analysis of the liquid-shell system. The coupling coefficients for the two shells under discussion are plotted in figure 4 as functions of frequency determinant size. (The results for the approximate solution are indistinguishable for $\beta = 0.044$, $\beta = 0.00044$.) Note the relatively small percent discrepancy (less than 6 percent except for Z_{22}) between the series and approximate solutions for the thinner shell and the only slightly increased discrepancy for the thicker shell.

This rather limited numerical investigation indicates that the convergence of the series solution can be expected to be good even for thin shells and that the approximate and series solutions differ by small percentages for thin shells and are, therefore, almost equally applicable. As the shell thickness increases (β increases), the discrepancy between the two solutions increases and the convergence and applicability of the series solution improve correspondingly.

EXPERIMENTAL OBJECTIVES

The experimental work was conducted to determine the dynamic properties of very thin liquid-filled cylindrical tanks subjected to axial vibration. The specific objectives were:

1. To determine the fundamental natural frequency of axisymmetric motion and the natural frequency of as many higher modes as feasible for various liquid levels and internal pressures,
2. To determine the frequency response curve for the fundamental axisymmetric mode indicating the ratio of internal pressure at tank bottom to tank base acceleration versus driving frequency,
3. To identify the asymmetric modes of vibration at several values of internal pressure and water level. This was done primarily to aid in distinguishing the symmetric modes from the asymmetric modes.

Test Specimens

The test specimens used in this study are shown in figure 5. The first specimen was a 5-inch-diameter, 6-inch-long, 0.001-inch-thick brass shim stock tank which was later replaced by a 0.0007-inch-thick electrodeposited nickel tank of the same dimensions. An 11-1/2-inch-diameter, 23-1/2-inch-long, 0.001-inch-thick brass shim stock tank was used in the final phase of testing. The specimen size and thickness affected the choice of test apparatus and equipment. The following factors were given primary consideration in selecting specimen and apparatus properties.

1. Very thin tanks are difficult to manufacture and handle, but have lower natural frequencies for a given tank size, or for a given natural frequency, the tank size is smaller.
2. A large tank size requires a larger shaker and support fixture, resulting in lower frequency elastic modes within the shaker-fixture system.
3. A large thin tank with the resulting lower natural frequency and higher mass permits better control of acceleration level and waveform at low acceleration levels.
4. A large thin tank has a low burst pressure; hence, permissible acceleration levels are low.
5. A low-frequency test range provides a better acceleration waveform from the shaker and less distortion of the waveform due to shaker-fixture dynamics.

The 11-1/2-inch-diameter specimen was selected as the best trade off among the above factors. The smaller tanks used in earlier tests were easier to fabricate and were intended as preliminary models to indicate problem areas in testing technique and data quality.

As shown in figure 5, the specimens were constructed with thick end flanges so that they could be attached to a base plate and fitted with a lid. The cylindrical shell was soldered directly to the end flanges, providing essentially a "built in" end condition, since it was not feasible or necessary to simulate the "pinned" end condition assumed in the analysis for such a thin shell. The base plates were designed to support the tank on the vibration fixture, to provide a pressure seal, and to carry pressure cells. The lids also served as pressure seals, and means for filling and pressurizing the tank.

Test Apparatus

The general arrangement of the test apparatus is shown in figure 6. An electrodynamic shaker driving a hydraulic "slip table" produced the unidirectional sinusoidal motion of the specimen. The tank was pressurized with a shop air supply through a mercury manometer. Before the tank was pressurized, the

water level was measured with a water manometer connected to the tank base. The weight of the support fixture, the moving element of the slip table, and the specimen were counterbalanced by means of a hanging weight and pulley arrangement using elastic "bungee" cord to isolate fixture motion from the weight.

Instrumentation

The instrumentation arrangement is shown in figure 7. A differential pressure cell in the center of the tank base plate sensed the difference between pressures at the bottom of the liquid and the airspace above the water. Two accelerometers at the tank base provided signals for controlling shaker amplitude and for measuring base acceleration. The use of dual accelerometers eliminated any interaction problem between the recording instruments and the shaker servo-control circuit. Lateral motion of the tank wall was detected by capacitive type noncontacting displacement probes. These probes were attached to an overhead mounting fixture that provided axial and rotary movement of the probes to any point on the tank surface.

Procedure

The test procedure was essentially the same for all specimens. First, the frequency of longitudinal motion was swept from 50 to 1200 cps for the 5-inch-diameter tanks and from 50 to 500 cps for the 11-1/2-inch-diameter tank for a number of water levels. These sweeps were intended to locate and identify as many system modes as possible. The acceleration level was varied initially to determine, by trial and error, a level for which subharmonic surface resonance and liquid surface instabilities (ref. 11) produced minimum distortion of acceleration and pressure signals. The upper limit of the acceleration level was of course determined by the requirement that peak pressures encountered at symmetric mode resonance be below the tank yield pressure.

The amplitudes of base acceleration, center pressure, and top acceleration, as well as phase angle relative to base acceleration, were recorded during each frequency sweep. Frequency sweeps were made for various values of internal pressure up to 1.5 psi for the large tank and 4 psi for the small tanks, and for various water levels from empty to full. Asymmetric modes were identified by rotating the displacement probes around the tank and noting the variation of wall motion amplitude as a function of angular position of the probe while frequency and base acceleration amplitude remained constant. These modes are easily identified since they characteristically exhibit an even number of peaks of radial displacement amplitude in 360° of rotation.

First symmetric mode frequency response data were obtained by sweeping the excitation frequency at a constant acceleration and observing base acceleration and pressure amplitudes. The response curve for the 5-inch-diameter tank was taken for the nearly full condition (approximately 1/2 inch below the tank lid), while the half full condition was used for the 11-1/2-inch-diameter tank.

RESULTS

The first symmetric mode frequency is plotted in figure 8 as a function of water level for 3.0 psig internal pressure for the 5-inch-diameter nickel tank. Figure 9 is a similar plot for the 11-1/2-inch-diameter tank with 1.0 psig internal pressure. In both figures, the theoretically predicted curves are shown for comparison. Figure 10 is a plot of the first symmetric mode frequency as a function of internal pressure for the 5-inch-diameter tank nearly full (approximately 1/2 inch of airspace above the water).

The experimental frequency response curves for the 5-inch-diameter and 11-1/2-inch-diameter tanks, respectively, are shown in figures 11 and 12. These curves show the ratio of pressure amplitudes at the center of the tank base to base acceleration as a function of driving frequency. For the 5-inch tank, the nearly full condition with 3.0 psig internal pressure was chosen, while a 12-inch water level and 1.0 psig internal pressure was used for the 11-1/2-inch-diameter tank response curve. In either case, water level, internal pressure, and acceleration level were chosen to yield the best data. Test conditions were selected by trial and error to obtain the set of conditions where acceleration and pressure waveforms showed the least distortion from subharmonic surface resonance, liquid surface instabilities, asymmetric breathing modes, and shaker-fixture dynamics. The extent of distortion appeared unpredictable, but certain combinations of test conditions yielded better waveforms than others.

These distortions were clearly caused, in part, by the subharmonic liquid surface resonance and capillary wave formation associated with breathing modes as reported by Kana, Lindholm, and Abramson (ref. 11). They also reported that, at certain acceleration levels, a jump phenomenon caused a sudden change in breathing mode response amplitude when the natural frequency was approached from below. The beat phenomenon (ref. 11) that involved a low frequency amplitude modulation of the pressure and radial wall displacement signals was also observed at certain frequencies. This amplitude modulation was always accompanied by a large, visible liquid surface motion and a modulation of the audible energy from the tank wall, both at the same frequency. No attempt was made to study these phenomena quantitatively because the test apparatus was inadequate for such an analysis and they were not important to the purpose of the present study.

The frequency spectrum of the most predominant asymmetric breathing modes for the 5-inch-diameter brass tank is plotted in figure 13. These modes were identified to determine when they were likely to distort the symmetric mode response.

Discussion of Experimental Results

The comparison of experimental and analytical frequency versus water level curves (fig. 8) indicates agreement within 10 percent for water levels above 2 inches. Below the 2-inch water level, however, the experimental

values of fundamental frequency are as much as 16 percent higher than predicted. For water levels above 3-1/2 inches, both fundamental and second mode data agree with predicted values within 2 percent.

The comparison of predicted and experimental frequency versus water level curves for the 11-1/2-inch-diameter tank (fig. 9) indicates agreement within 5 percent for all data obtained. Data for water levels above 14 inches were not obtained because the test specimen ruptured accidentally at that point. Attempts to locate the fundamental frequency at water levels below 4 inches were unsuccessful because the distortion of both acceleration and pressure signals was high throughout the frequency spectrum. Testing with a new specimen at higher water levels was discontinued since the data of both figures 8 and 9 indicated very good agreement between prediction and experiment at higher water levels.

The measured variation of fundamental natural frequency with internal pressure (fig. 10) indicates a frequency change of approximately 2 percent as the pressure varies from 1 to 4 psi, which agrees with the theoretical result that frequency is essentially independent of internal pressure (see eq. (20')). Data from the other two specimens also indicate that frequency is essentially independent of internal pressure.

The frequency response curves of figures 11 and 12 indicate that the test system behaves essentially as a linear single-degree-of-freedom system near the fundamental frequency. The amplification factor was not calculated since no attempt was made to assess system damping.

The natural frequencies of symmetric modes of the liquid-tank system were difficult to determine primarily because of the presence of other phenomena (ref. 11) that distorted the symmetric mode motion. The excitation of asymmetric tank breathing modes at frequencies very near symmetric mode frequencies was almost unavoidable partly because these breathing modes are capable of subharmonic excitation. Large amplitude breathing mode motion at 1/2 and 1/3 harmonics was not uncommon and it is suspected that even lower harmonics were present although they could not be clearly identified. The fact that breathing mode frequencies vary with pressure, however, while the symmetric mode frequencies are essentially independent of pressure provided a means of isolating the symmetric modes. Another phenomenon that caused difficulty, primarily in attempting to establish precise pressure-to-acceleration-amplitude ratios, was the frequency modulation of symmetric mode motion at the same frequency as some low frequency liquid surface mode. This phenomenon was more pronounced at higher acceleration levels and resulted in large surface motions. A difficulty which arose from the test apparatus configuration was that of producing a pure sinusoidal axial motion of the tank base as a rigid plate. This became impossible at higher test frequencies where the inevitable deformations of the base undoubtedly excited unwanted system modes. As mentioned earlier, this problem would be difficult to remedy because, even though larger tanks have lower frequencies, base flexibility also increases with tank size.

CONCLUDING REMARKS

A comparison of the two theoretical solutions demonstrated that the series and one-term approximate solutions are equally applicable for thin shells; however, the ease of application of the approximate solution warrants its use. As the shell thickness-to-radius ratio becomes larger, the series solution converges more rapidly while the accuracy of the approximate solution deteriorates.

The experimental results of this study indicate that the theory does, in fact, provide a good mathematical model for thin shells filled with liquid. The best agreement between theory and experiment was obtained for liquid depths greater than the radius of the shell, indicating that surface dynamics should be included for lower liquid levels.

It should not be overlooked that this study attempts to explain only one of the physical phenomena associated with the vibration of liquid filled elastic tanks subjected to axial excitations. In fact, as demonstrated in the experimental phase, it is often difficult to isolate this particular phenomenon. This analysis is useful, however, in problems where the primary concern is the force transmitted across the tank bottom (i.e., longitudinal dynamics of a missile) and not the local motion of the fluid flow (sloshing).

Ames Research Center
National Aeronautics and Space Administration
Moffett Field, Calif., Nov. 3, 1966
124-11-05-03-21

REFERENCES

1. Bleich, H. H.: Longitudinal Forced Vibrations of Cylindrical Fuel Tanks. Jet Propulsion, vol. 26, no. 2, Feb. 1956, pp. 109-111.
2. Lianis, G.; and Fontenot, L. L.: Analysis of the Free Vibrations of Pressurized Cylindrical Shells Filled With an Ideal Liquid Having a Free Surface. Rep. No. ERR-AN-194, General Dynamics Astronautics, Sept. 1962.
3. Abramson, H. N.; Kana, D. D.; and Lindholm, U. S.: Breathing Vibrations of a Circular Cylindrical Shell Containing an Internal Liquid. Tech. Rep. No. 3, Southwest Research Institute, Texas, Feb. 1, 1962.
4. Mixson, J. S.; and Herr, R. W.: An Investigation of the Vibration Characteristics of Pressurized Thin-Walled Circular Cylinders Partially Filled With Liquid. NASA TR R-145, 1962.
5. Shmakov, V. P.: The Equations of the Axially Symmetric Vibrations of a Liquid-Filled Cylindrical Shell. NASA TT F-219, 1964.
6. Saleme, E.; and Liber, T.: Breathing Vibrations of Pressurized Partially Filled Tanks. AIAA J., vol. 3, no. 1, Jan. 1965, pp. 132-136.
7. Abramson, H. N.: Dynamic Behavior of Liquid in Moving Container. Appl. Mech. Rev., vol. 16, no. 7, July 1963, pp. 501-506.
8. Kana, D. D.: Longitudinal Forced Vibration of Partially Filled Tanks. Tech. Rep. No. 6, Southwest Research Institute, Texas, 1963.
9. Lamb, Horace: Hydrodynamics. Sixth ed., Dover Publications, 1945.
10. Timoshenko, S.: Theory of Elastic Stability. McGraw-Hill Book Co., Inc., 1936.
11. Kana, D. D.; Lindholm, U. S.; and Abramson, H. N.: An Experimental Study of Liquid Instability in a Vibrating Elastic Tank. Tech. Rep. No. 5, Southwest Research Institute, Texas, Jan. 31, 1963.

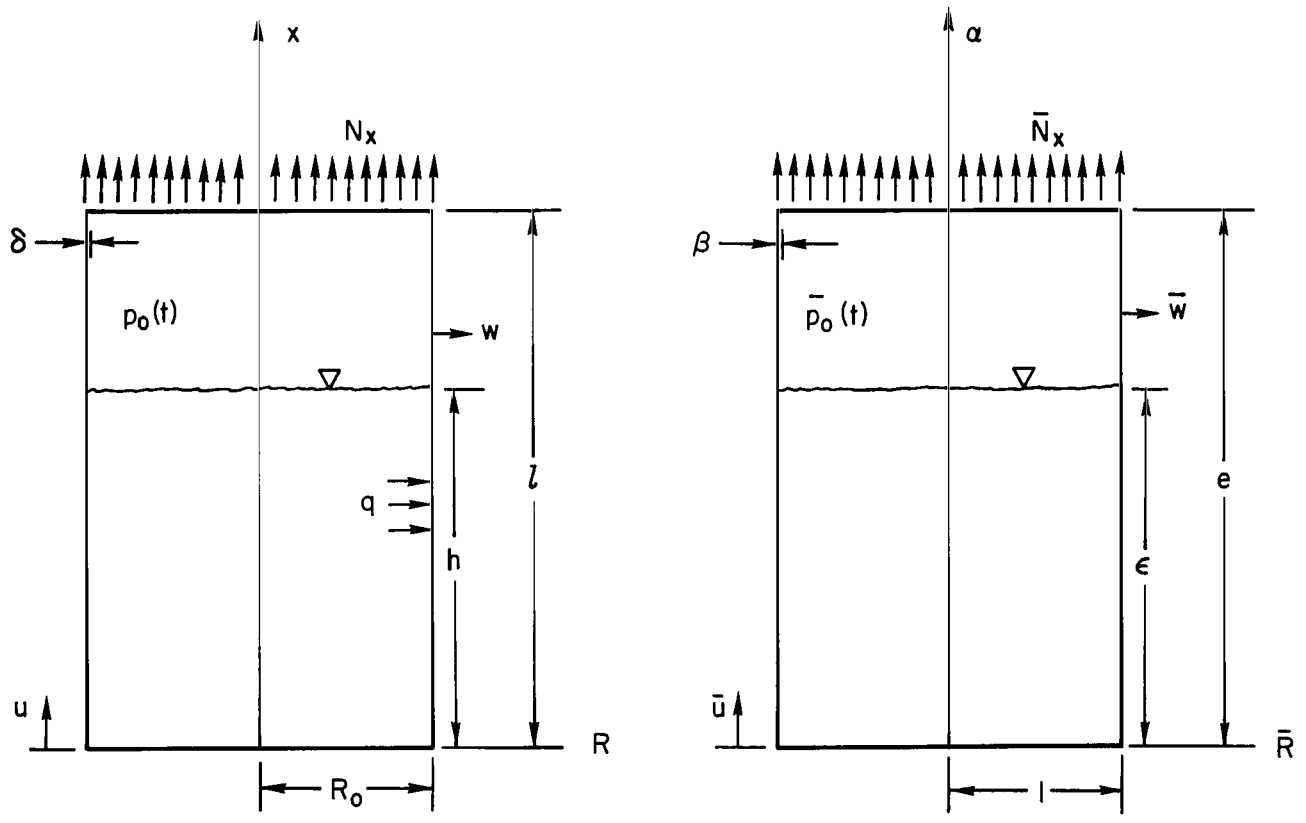


Figure 1.- Liquid-shell geometry and coordinate system.

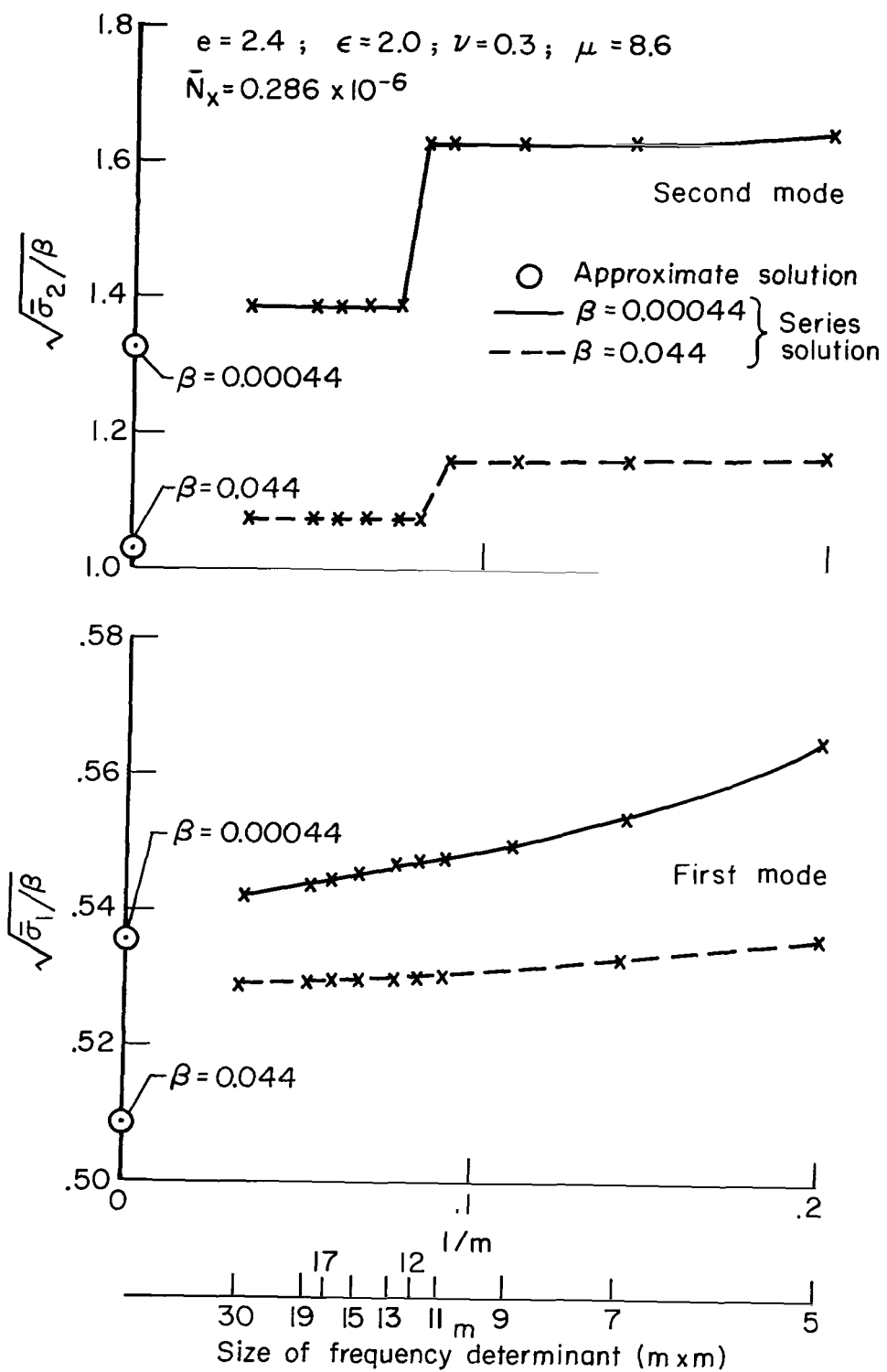


Figure 2.- Frequency parameter.

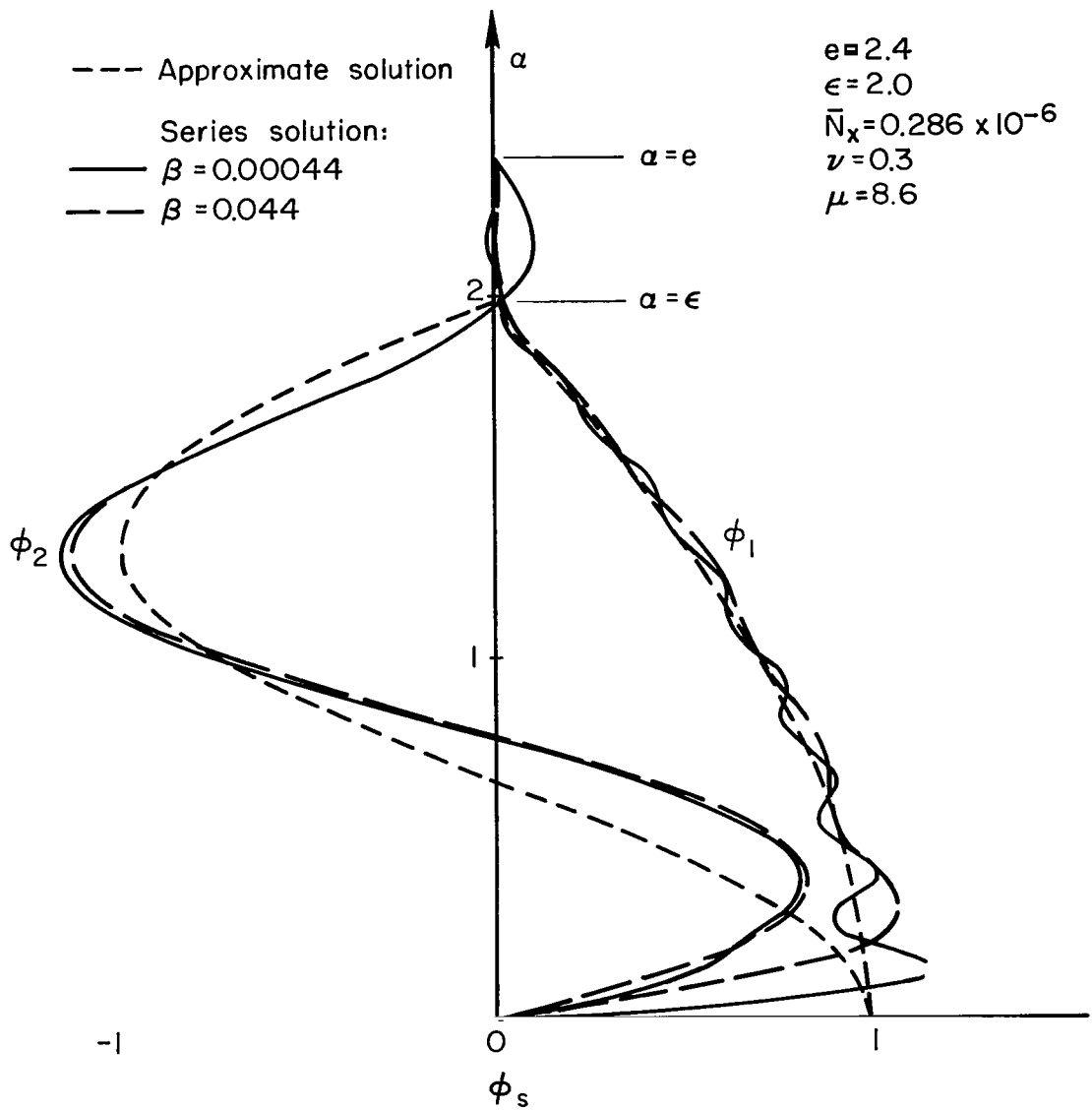


Figure 3.- Mode shapes.

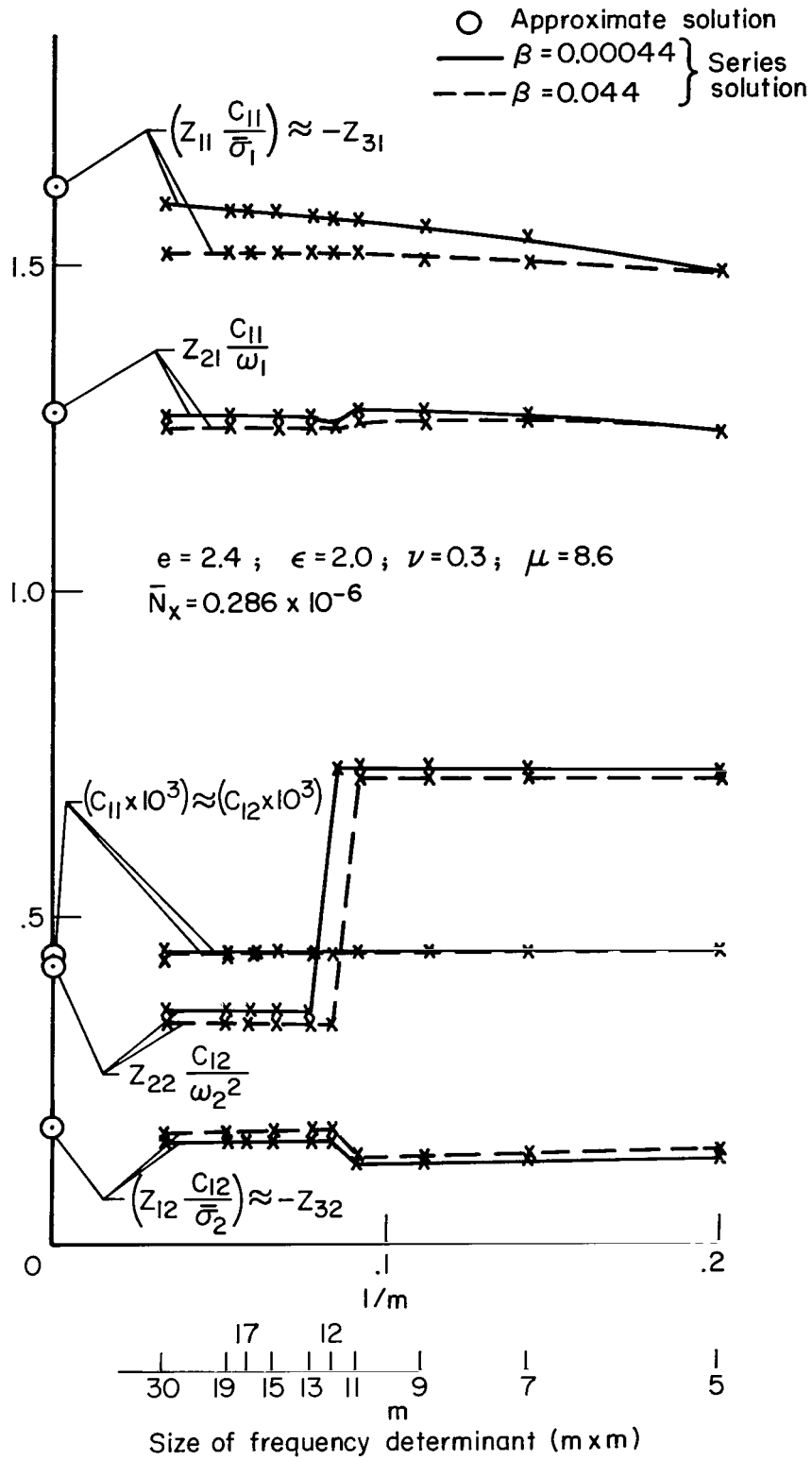
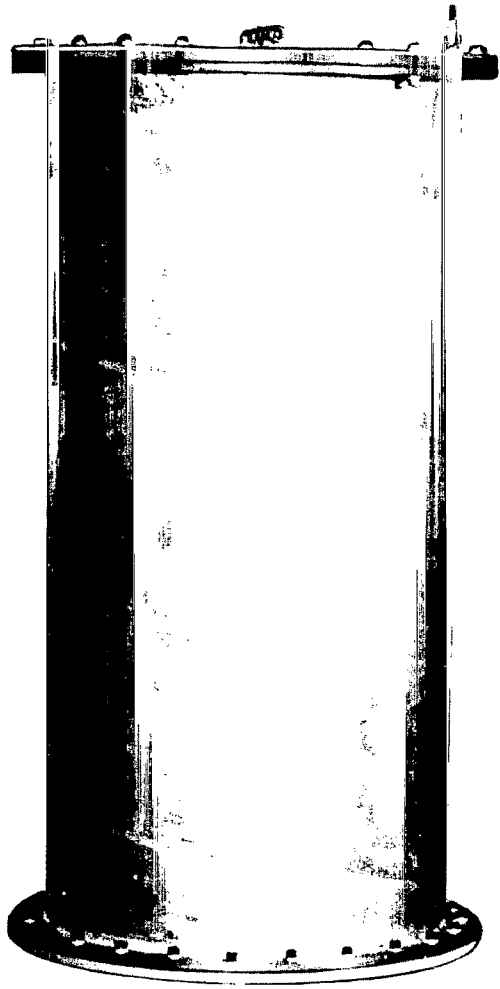
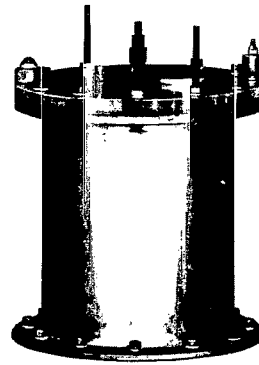


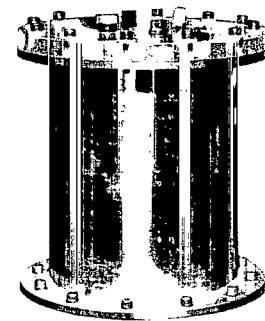
Figure 4.- Coupling coefficients.



1 1/2-inch-diameter brass tank



5-inch-diameter nickel tank



5-inch-diameter brass tank

A-37005

Figure 5.- Test specimens.

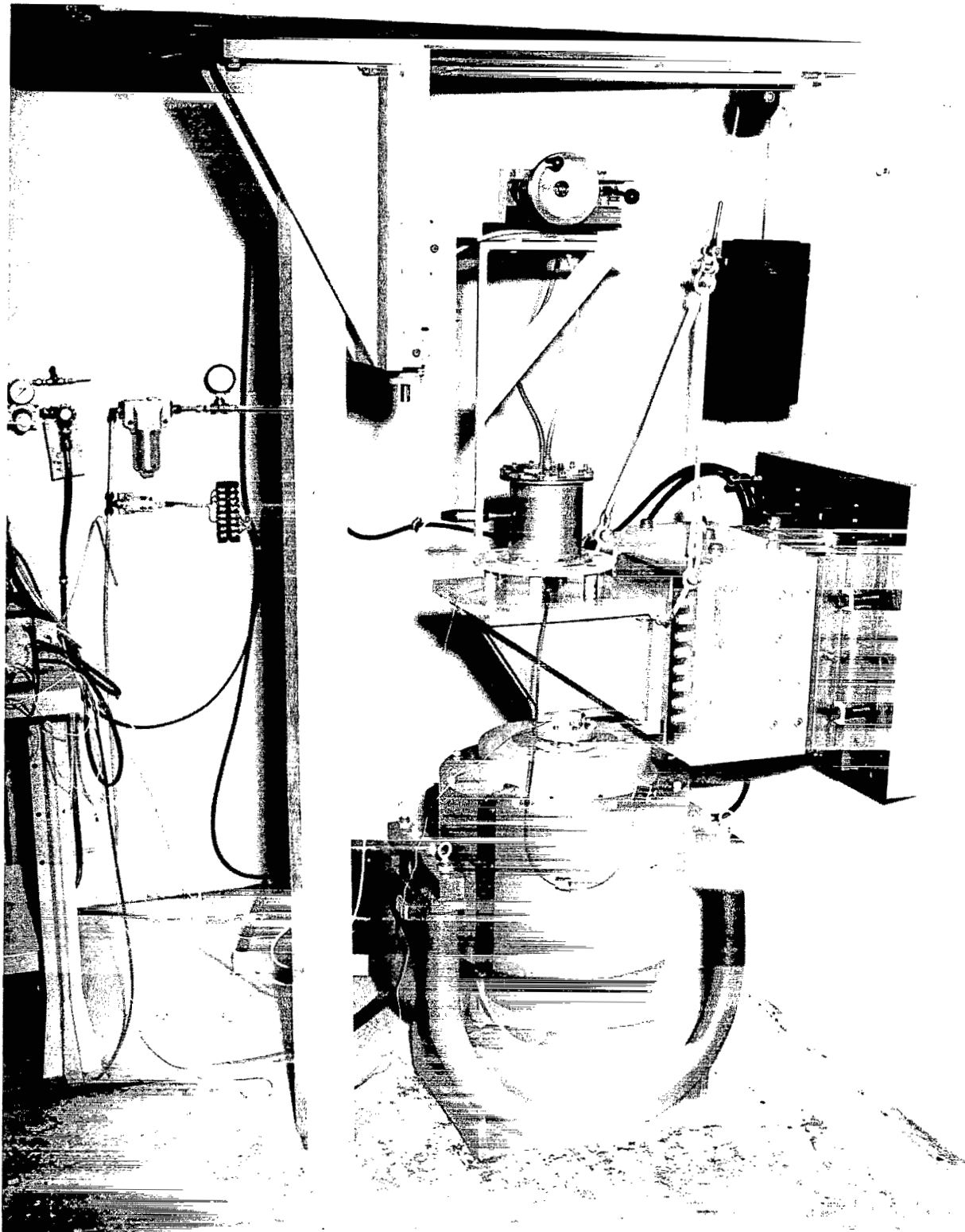


Figure 6.- Test apparatus.

A-36083

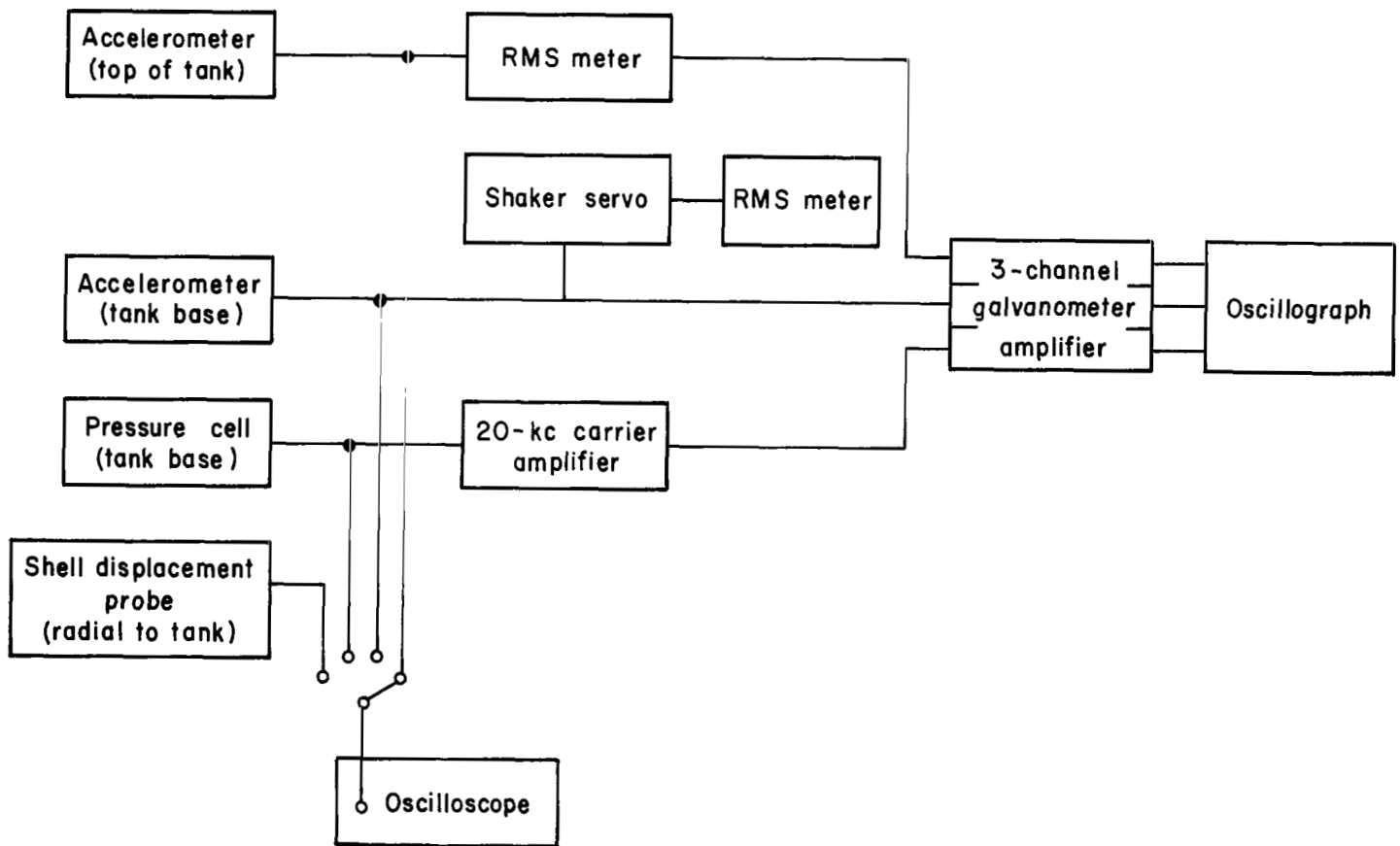


Figure 7.- Instrumentation arrangement.

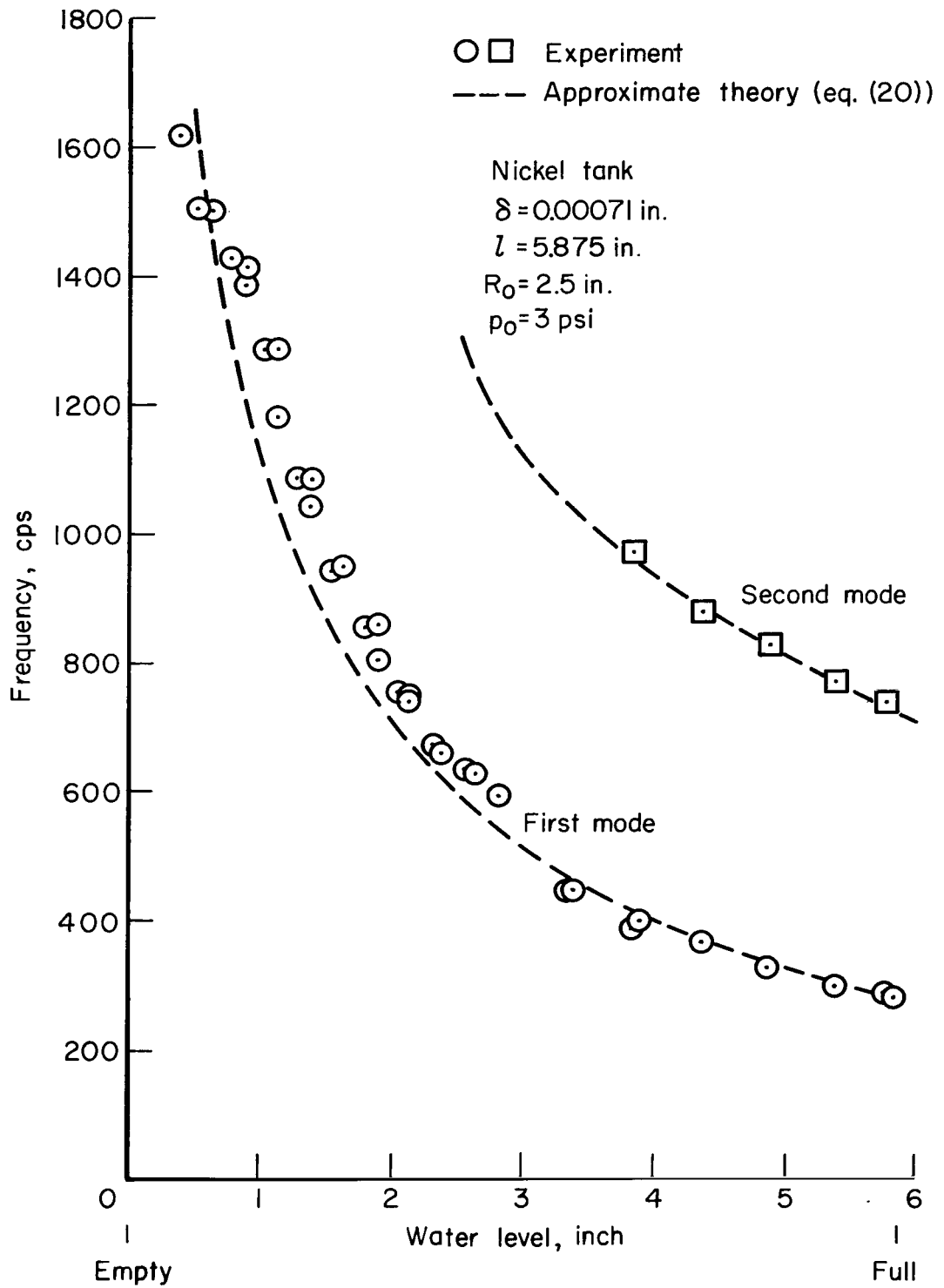


Figure 8.- Nickel tank natural frequency versus water level.

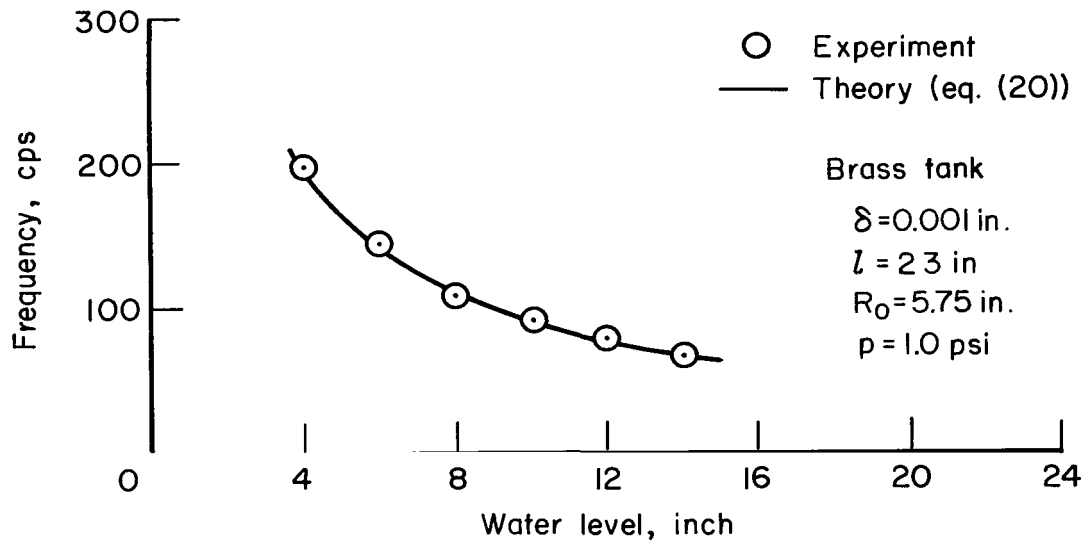


Figure 9.- First symmetric mode frequency versus water level.

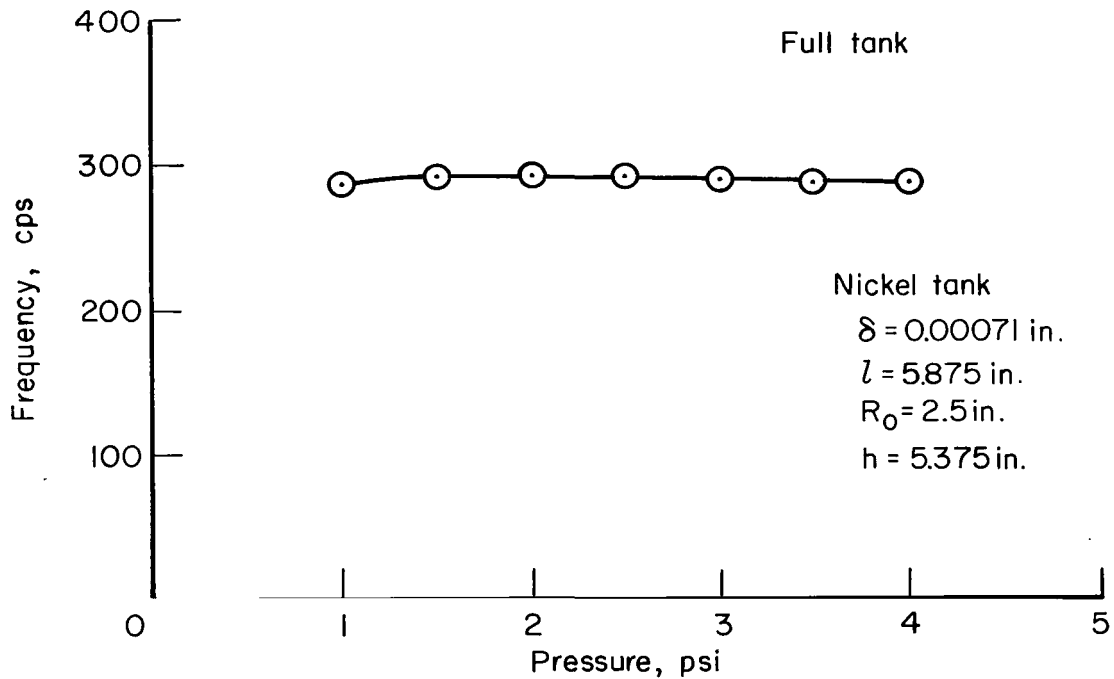


Figure 10.- Variation of fundamental symmetric frequency with tank pressure.

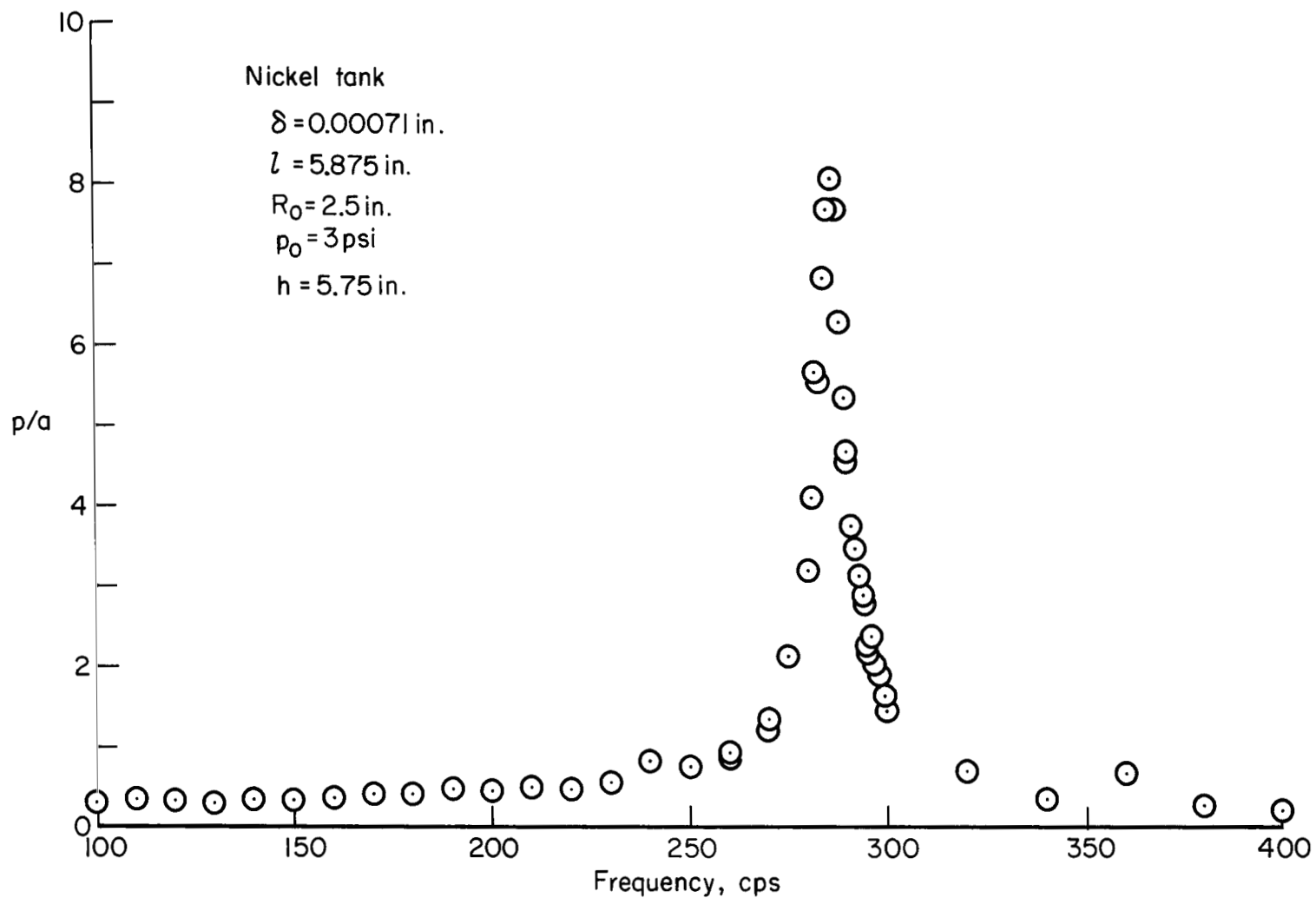


Figure 11.- Fundamental symmetric mode frequency response, nickel tank.

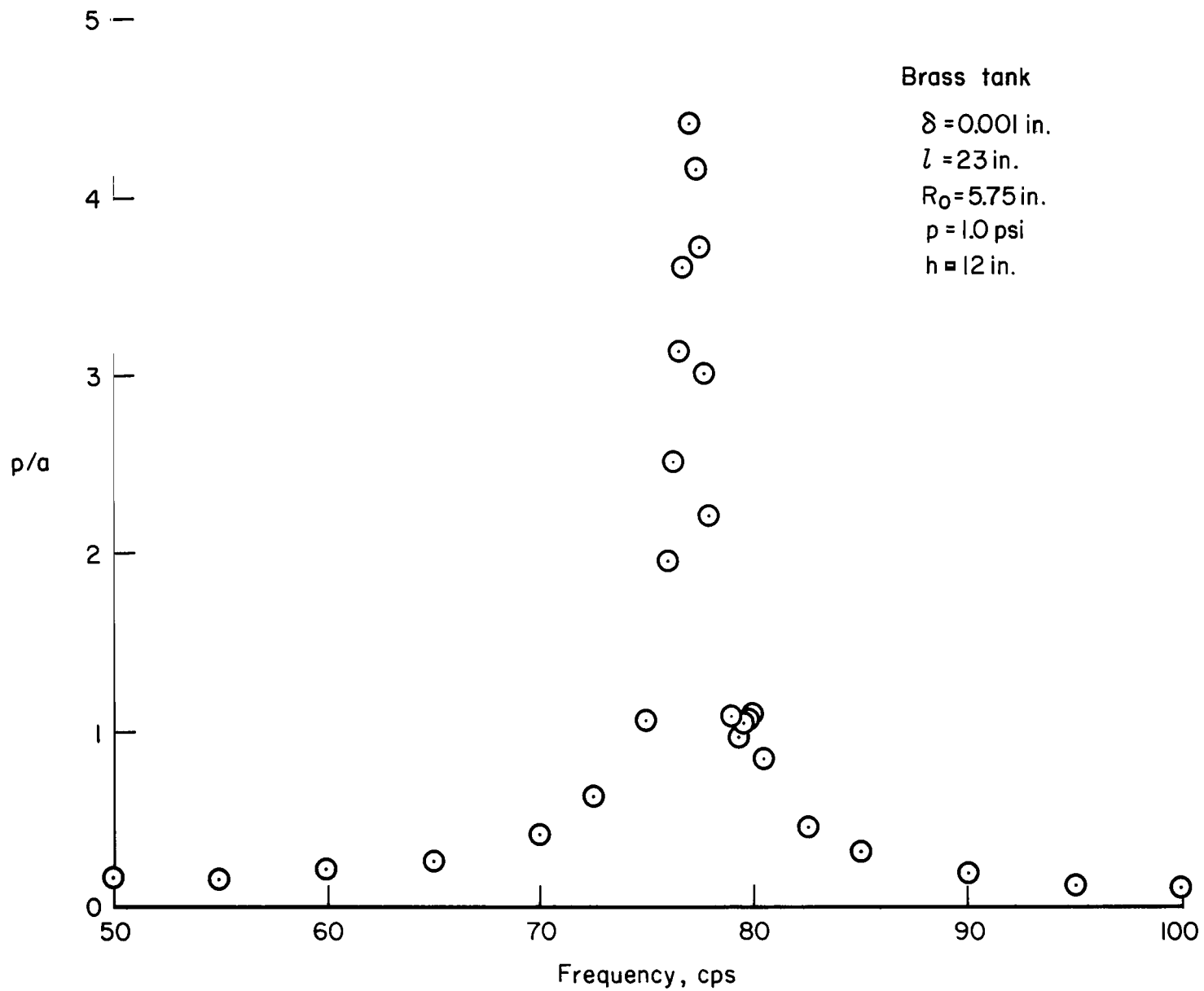


Figure 12.- Fundamental symmetric mode frequency response, brass tank.

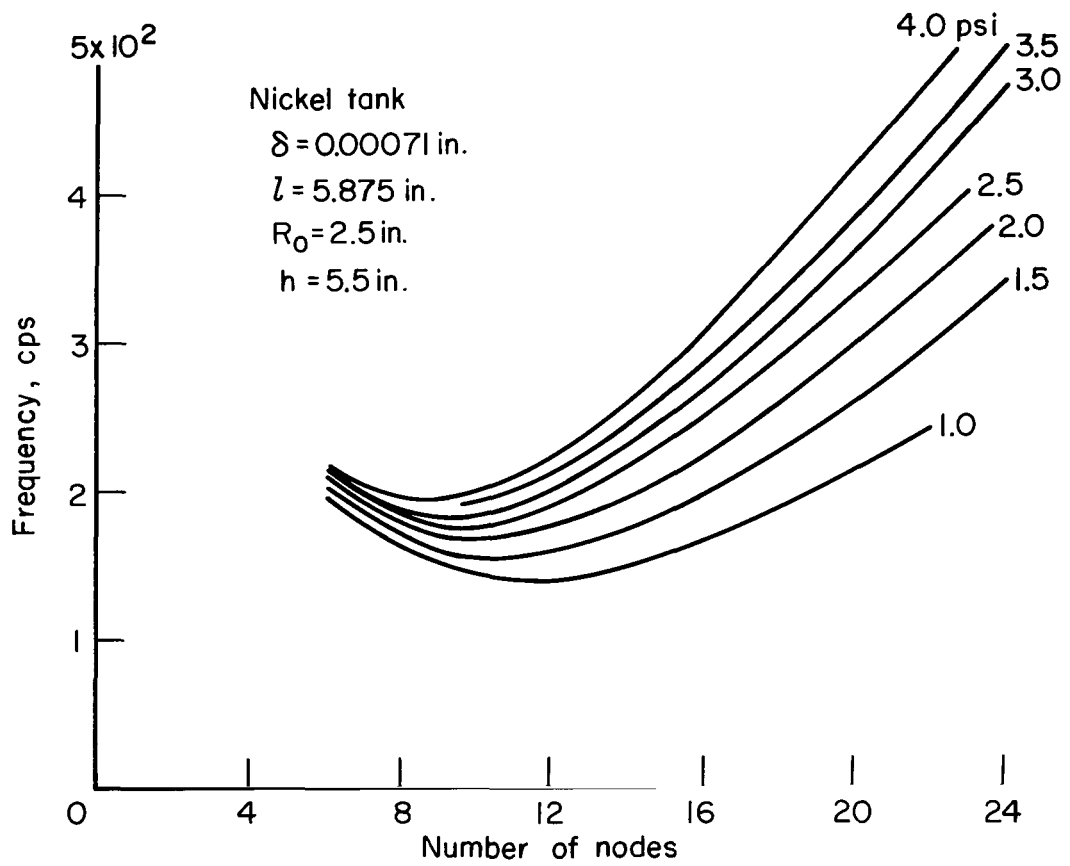


Figure 13.- Location of asymmetric modes in frequency spectrum.

"The aeronautical and space activities of the United States shall be conducted so as to contribute . . . to the expansion of human knowledge of phenomena in the atmosphere and space. The Administration shall provide for the widest practicable and appropriate dissemination of information concerning its activities and the results thereof."

—NATIONAL AERONAUTICS AND SPACE ACT OF 1958

NASA SCIENTIFIC AND TECHNICAL PUBLICATIONS

TECHNICAL REPORTS: Scientific and technical information considered important, complete, and a lasting contribution to existing knowledge.

TECHNICAL NOTES: Information less broad in scope but nevertheless of importance as a contribution to existing knowledge.

TECHNICAL MEMORANDUMS: Information receiving limited distribution because of preliminary data, security classification, or other reasons.

CONTRACTOR REPORTS: Technical information generated in connection with a NASA contract or grant and released under NASA auspices.

TECHNICAL TRANSLATIONS: Information published in a foreign language considered to merit NASA distribution in English.

TECHNICAL REPRINTS: Information derived from NASA activities and initially published in the form of journal articles.

SPECIAL PUBLICATIONS: Information derived from or of value to NASA activities but not necessarily reporting the results of individual NASA-programmed scientific efforts. Publications include conference proceedings, monographs, data compilations, handbooks, sourcebooks, and special bibliographies.

Details on the availability of these publications may be obtained from:

SCIENTIFIC AND TECHNICAL INFORMATION DIVISION
NATIONAL AERONAUTICS AND SPACE ADMINISTRATION
Washington, D.C. 20546